IEEE Access
Multidisciplinary ⋮ Rapid Review ⋮ Open Access Journal

Received September 24, 2020, accepted October 7, 2020, date of publication October 12, 2020, date of current version November 6, 2020.

Digital Object Identifier 10.1109/ACCESS.2020.3030271

Hard-Division and Multi-Model Based Floating Height Prediction for Air Cushion Furnace With Hybrid Nozzles

SHUAI HOU[1], XIAOLIN HAN[1], XINYUAN ZHANG[1], MEIJUAN BAI[1], AND FUAN HUA[2]

[1]School of Information and Electrical Engineering, Hebei University of Engineering, Handan 056038, China
[2]State Key Laboratory of Rolling and Automation, Northeastern University, Shenyang 110819, China

Corresponding authors: Meijuan Bai (baimeijuan@hebeu.edu.cn) and Fuan Hua (huafa@ral.neu.edu.cn)

This work was supported in part by the National Natural Science Foundation of China under Grant 61973306 and Grant 61802107, in part by the Open Project Foundation of the State Key Laboratory of Synthetical Automation for Process Industries under Grant PAL-N201706, in part by the Natural Science Foundation of Hebei Province under Grant E2017402115, in part by the Science and Technology Innovation Fund of Dalian under Grant 2020JJ26GX040, in part by the Fundamental Research Funds for the Central Universities under Grant DUT20JC19, and in part by the National Key Research and Development Program of China: Energy Consumption Analysis and Optimization Control Software for Construction Machinery under Grant 2020YFB1709900.

ABSTRACT The strip floating height is a key factor affecting production efficiency and quality of the air cushion furnace. At present, the air cushion furnace with hybrid nozzles is the most typical heating and drying equipment. In order to predict the floating height of the strip in this equipment, a hard-division and multi-model based floating height prediction method is proposed. In hard division method, the process is divided into several stable and vibration stages. On the one hand, time interval based novel density clustering algorithm is proposed so as to avoid the wrong division caused by noise at hard division stage. On the other hand, covariance matrices based local density is presented to better capture dynamic characteristics of the process. In the multi-model stage, a hybrid prediction model under stable state and XGBoost-based model under vibration state are established to predict the strip floating height. The hybrid prediction model is composed of mechanism model and data driven model. The mechanism model is proposed by combining the force balance equation and inviscid theory which can predict the major information of the floating height and the data driven model compensates the error of the mechanism model. A mount of experiments have been carried out on the existing air cushion experimental platform and show desirable prediction effect.

INDEX TERMS Air cushion furnace with hybrid nozzles, floating height, hard division, hybrid prediction model.

I. INTRODUCTION

The high quality metal strips, such as aluminum auto body sheet (ABS), aviation aluminum-alloy, high precision electronic copper strip, and silicon steel, etc., are widely used in the high-end manufacturing industry, power industry, and information technology industry [1], [2]. The production process of strips needs to meet three technological requirements: a) high heating efficiency, b) high temperature uniformity, and c) contactless heat treatment [3]. With the high heating efficiency, temperature control precision and product surface quality, the air cushion furnace becomes an indispensable equipment in the production process of the high quality metal strips [4].

According to different structures, the air cushion furnaces can be classified into three categories: air cushion furnaces with slot nozzles [5], air cushion furnaces with round nozzles [6], [7], and air cushion furnaces with hybrid nozzles combining slot and round nozzles [8]. The air cushion furnace with hybrid nozzles has great impinging force and high heat transfer efficiency [8]. However, until now, researches have not found out the floating height prediction of the strip in the air cushion furnace with hybrid nozzles.

During the working process of the air cushion furnace, the strip is supported by the gas ejected from the nozzles and floats in the furnace to ensure the surface quality of the strip. However, if the floating height exceeds a reasonable range, the surface of the strip may contact with nozzles and be scratched. Besides, the floating height impacts the heating and drying efficiency as well as the tension control of the whole production line. Hence, the floating height is a key factor affecting product quality. But it is difficult to measure the floating height of the strip due to the high temperature production environment [9]. In addition, the floating height of

The associate editor coordinating the review of this manuscript and approving it for publication was Xiao-Sheng Si.

the strip is affected by the floating states. The strip shows two floating states with different mechanism properties, stable state and vibration state [10]. Therefore, it is of great practical significance to construct a floating height prediction model for the air cushion furnace with hybrid nozzles.

In the past decades, several studies have been reported on floating heights under stable state. For example, Hornig *et al.* [11] studied the relationship between the floating height and the pressure coefficient through the numerical simulation method. Moretti developed the governing Partial Differential Equations to predict the floating height of strip [12]. Cho used the flexible cantilever beam and ground effect theory to formulate the mechanism model of floating height [13]. However, the above researches were carried out by means of the numerical simulation or the mechanism modeling. The mechanism modeling method has advantages of strong physical interpretation ability and generalization. But it is often constructed on the basis of certain ideal assumptions so that it is difficult to obtain the expected prediction accuracy. In view of the strong learning ability of data driven model, Hou constructed a parallel hybrid model combining the mechanism model with the data driven model to predict the floating height in the air cushion furnace with slot nozzles-[14], [15]. But this proposed model is not suitable for air cushion furnace with hybrid nozzles due to the different structure of the air cushion furnace. Chang and Moretti [16] analyzed the aerodynamic characteristics by means of the ground effect theory in the hybrid nozzle. However, the prediction of the floating height in the hybrid nozzle structure was not studied in the literature.

Additionally, in vibration state, Cho established a vibration model on the basis of the elastic equation and the discrete model [13]. Takeda and Watanabe established a self-excited vibration model according to the equations of the strip motion, the fluid force and energy balance [10]. However, the mechanism models of the above works are established based on certain ideal assumptions. Thus they have poor prediction effect and only can be used under some specific conditions. Compared with mechanism model, data driven model is easier to construct and has higher prediction accuracy. They are often used to solve the problem of vibration signal prediction in industrial processes. Hou used the least square support vector regression (LSSVR) to predict the maximum and minimum floating height of the strip in the air cushion furnace with double-slot nozzle and obtained good prediction results [14]. Due to the advantages of efficiency, flexibility and scalability, eXtreme Gradient Boosting (XGBoost) is often used in the prediction of vibration signals in the other fields of industry [17]–[20].

In fact, different states have distinct process correlation characteristics, so a single model cannot accurately describe the whole multi-state process. Hou *et al.* [14] proposed a state division method based on K-means clustering algorithm. This method depends heavily on the selection of the initial clustering center. Zhao and Sun [21] and Hou *et al.* [15] proposed the stage division methods on the basis of the multivariate statistical methods and obtained the desirable effect in multi-state industrial processes. However, the partition results are greatly affected by the relaxation factor which is turned by artificial experience. According to this problem, an iterative two-step sequential phase partition (ITSPP) method based on density peaks clustering (DPC) algorithm was proposed by Qin *et al.* [22]. But DPC relies heavily on cutoff distance and does not consider the local structure of the data. To overcome these problems, Du *et al.* [23] proposed the density peaks clustering based on k nearest neighbors (DPC-KNN). However, on the one hand, the use of Euclidean distance in k nearest neighbors cannot accurately measure the relationship between data and express the process variable correlations. On the other hand, these methods do not consider the influence of time sequence and may misclassify the noise samples as normal samples. By comparison, covariance matrix can better capture the dynamic characteristics of process [24]. In addition, it has been proved that the effect of stage division can be improved by introducing time intervals [25].

For the air cushion furnace with hybrid nozzles, a hard-division and multi-model based floating height prediction method is proposed in this article. The main contributions of this article can be described as follows: 1) To avoid wrong division caused by noise, a novel density clustering algorithm based on time interval is proposed to divide the process into stable states and vibration states. 2) A covariance matrices based local density for the novel density clustering algorithm is presented to better capture the process dynamic characters. 3) For the hybrid nozzle structured air cushion furnace under stable state, a hybrid model composed of a mechanism model and a data model is proposed to predict the floating height. The hybrid model can combine the strong learning ability of data driven model and highly robust of the mechanism model.

The remainder of this article is organized as follows. In section II, air cushion furnace with hybrid nozzles and the density clustering algorithm are briefly introduced. In section III, the proposed hard division method is described in detail. In section IV, the hybrid prediction model under stable state and the XGBoost-based model under vibration state are illustrated. Section V details the experiments and analysis. Conclusions are given in section VI.

II. PRELIMINARY KNOWLEDGE

A. AIR CUSHION FURNACE WITH HYBRID NOZZLES

The structure of the air cushion furnace with hybrid nozzles is shown in Fig. 1(a). There are several upper air boxes with hybrid nozzles at the top of the air cushion furnace and several lower air boxes with hybrid nozzles at the bottom of the air cushion furnace. The strip floats between the upper and lower air boxes in the production process. For the convenience of the reader, the enlarged schematic diagram of hybrid nozzles is shown in the Fig. 1(b). Every hybrid nozzle has two slot nozzles and two rows of round nozzle located between the two slot nozzles as sketched in Fig. 2.

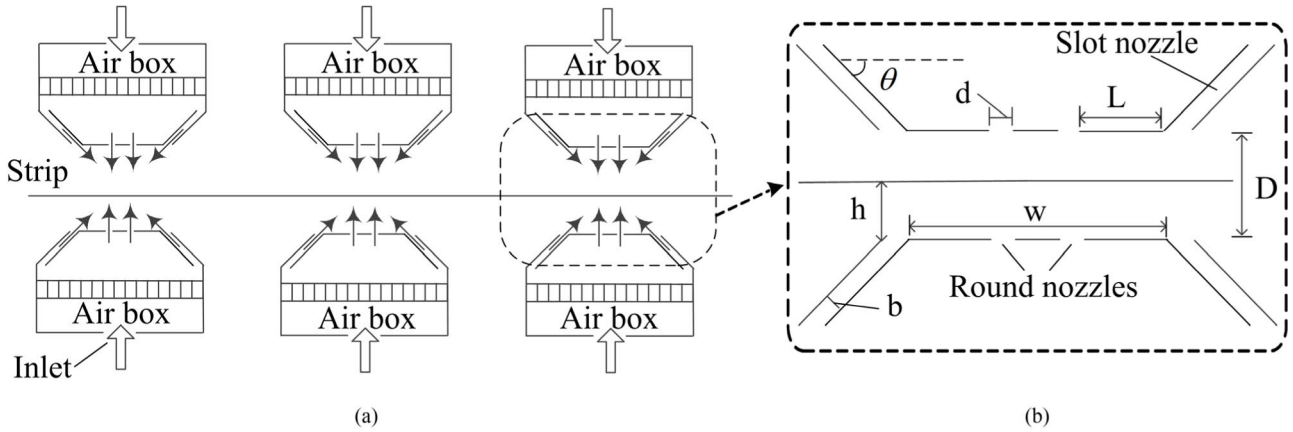

FIGURE 1. Schematic of the hybrid nozzles in air cushion furnace: (a) Schematic of the strip floating at stable state; (b) The partial enlarged drawing of nozzle.

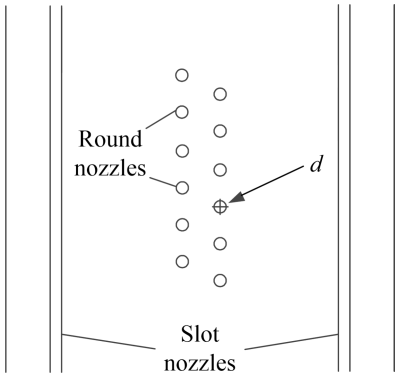

FIGURE 2. Top view of the hybrid nozzles.

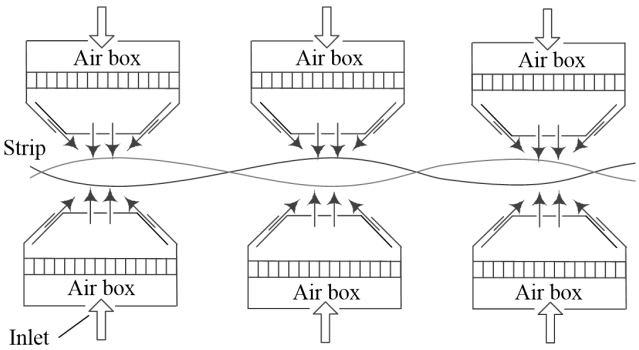

FIGURE 3. Schematic of the strip floating at vibration state.

The working process is shown in Fig. 1(a). As the arrows indicate in Fig. 1(a), the air enters from the inlet of the air box and flows out the nozzle, and then impinges on the strip surface during the production process. The strip floats in the air under the impinging force of the upper and lower nozzle in stable state or vibration state. The stable state of the strip refers to the state where the strip is located at the mechanical equilibrium point and its floating height hardly changes over time, as shown in Fig. 1(a). Moreover, the vibration state of the strip indicates the state that the strip floats up and down over time, as shown in Fig. 3.

In order to facilitate the calculation of the later formula, the related variables are defined in Table 1.

B. DENSITY CLUSTERING ALGORITHM

The clustering algorithms can be divided into four categories, such as partition-based clustering method, density-based clustering method, hierarchy-based clustering method, and grid-based clustering method [26]–[31]. Density peaks clustering (DPC) algorithm is proposed by Alex Rodriguez and Alessandro Laio in 2014 [32].

For data set $X = \{x_i\}\,(i \in [1, N])$, local density ρ_i is expressed as:

$$\rho_i = \sum\nolimits_j \chi(d_{ij} - d_c), \tag{1}$$

where d_{ij} is the distance between the data point x_i and x_j, d_c is cutoff distance, and χ is a function, which can be given by:

$$\chi(x) = \begin{cases} 1, & if\ x < 0 \\ 0, & if\ otherwise. \end{cases} \tag{2}$$

The distance δ_i is the mapping function of ρ_i, which is defined as:

$$\delta_i = \begin{cases} \min_{\rho_j > \rho_i}(d_{ij}), & \rho_i \neq \max_{i=1\ldots N}(\rho_n) \\ \max(d_{ij}), & \rho_i = \max_{i=1\ldots N}(\rho_n). \end{cases} \tag{3}$$

Finally, the number of clusters can be determined by the two-dimensional decision graph of ρ and δ.

The DPC algorithm is not fully suitable for industrial scenarios. There are two main reasons. On the one hand, in industrial scenarios, data is often collected in the order of time and the sampling time is an important and useful variable for the analysis of industry process [25]. On the other hand, the Euclidean distance cannot accurately reflect the relationship between the samples on the industrial data set,

TABLE 1. Nomenclature.

Symbol	Description
D	gap between upper and lower air boxes
b	width of slot nozzle
d	diameter of round nozzle
w	distance between two slot nozzles
L	distance between slot nozzle and the closest row of round nozzles
θ	angle of slot nozzle
h	floating height; distance between strip and lower air box
p_c	air cushion pressure
p_{c1}	air cushion pressure of lower surface of strip
p_{c2}	air cushion pressure of upper surface of strip
p_t	pressure of air jet after slot nozzle
p_{t1}	pressure of the air jet after the lower slot nozzle
p_{t2}	pressure of the air jet after the upper slot nozzle
F	air impinging force per unit length
F_U	upward air impinging force per unit length
F_D	downward air impinging force per unit length
Δp_1	pressure drop between strip and round nozzle
Δp_{U1}	pressure drop between strip and lower round nozzle
Δp_{D1}	pressure drop between strip and upper round nozzle
ρ_*	air density
N	number of round nozzles in each row of round nozzles per unit length of air box
C_d	discharge coefficient
μ	dynamic viscosity of air
G	gravity of strip per unit length

which may deteriorate the effect of clustering. In addition, compared with the Euclidean distance, the covariance matrix can better capture the dynamic characteristics of industry process and get desirable results [24].

III. TIME INTERVAL AND COVARIANCE MATRICES DENSITY CLUSTERING BASED HARD DIVISION (TICMDC-HD)

In this section, a time interval and covariance matrices density clustering based hard division method (TICMDC-HD) is proposed. In order to capture dynamic characteristics in dynamic process and avoid the wrong division caused by noise, a local density ρ_i based on covariance matrices and distance δ_i based on time interval are proposed, -respectively. The establishment of covariance matrices is shown in Fig. 4.

In Fig. 4, a two-dimensional data set $X\ (I \times J)$ is collected in the production process of the air cushion furnace in chronological order. The parameter I is the number of samples and J is the number of variables, and x_i is a sample in $X\ (I \times J)$. At first, a data matric W_i is established by several continuous and adjacent samples x_i. The construction method of data

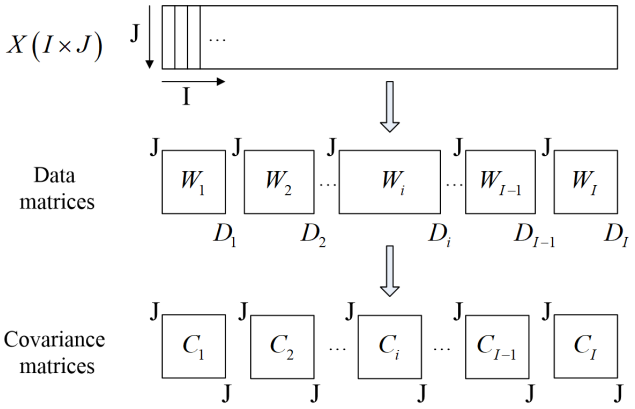

FIGURE 4. Schematic diagram of data matrices construction and transformation.

matric W_i is formulated by:

$$W_i = \begin{cases} [x_1, \ldots, x_{i+M}]^T, & 1 \le i \le M \\ [x_{i-M}, \ldots, x_{i+M}]^T, & M < i \le I - M \\ [x_{i-M}, \ldots, x_I]^T, & I - M < i \le I, \end{cases} \tag{4}$$

where M is a positive integer. The parameter D_i is the length of W_i, which can be further expressed as:

$$D_i = \begin{cases} i + M, & 1 \le i \le M \\ 2M + 1, & M < i \le I - M \\ I - i + M + 1, & \mathrm{I} - M < i \le I. \end{cases} \tag{5}$$

The covariance matrices C_i of each data matric W_i are calculated and the similarity $Cov_{i,i'}$ between two covariance matrices of samples is defined as:

$$Cov_{i,i'} = \sum_{p=1}^{J} \sum_{q=1}^{J} |C_i(p,q) - C_{i'}(p,q)|, \tag{6}$$

where p and q is the rows number and column number. i is the i^{th} sample and i' is another sample.

The local density ρ_i is defined as:

$$\rho_i = \exp\left(-\frac{1}{k}\sum_{i'=1}^{k} Cov_{ii'}^2\right), \tag{7}$$

where k is the predefined number of nearest neighbor samples.

The factor of time interval between two samples is also introduced to the distance δ_i. The distance δ_i of each sample is expressed as:

$$\delta_i = \begin{cases} \min_{\rho_{i'} > \rho_i}(Cov_{ii'} + \Delta t_{ii'}), & \rho_i \ne \max_{i=1\ldots I}(\rho_{i'}) \\ \max(Cov_{ii'} + \Delta t_{ii'}), & \rho_i = \max_{i=1\ldots I}(\rho_{i'}), \end{cases} \tag{8}$$

where $\Delta t_{ii'}$ represents the absolute value of time interval between x_i and $x_{i'}$. In order to suppress the adverse effects brought by the value difference between $Cov_{i,i'}$ and $\Delta t_{ii'}$. The $Cov_{i,i'}$ and $\Delta t_{ii'}$ should be normalized.

The TICMDC-HD is described in detail as follows:

Input: data set X $(I \times J)$, $\Delta t_{ii'}(i = 1, \ldots, I, i' = 1, \ldots, I)$, the number of nearest neighbors k, the geometric centers c_s and c_v of historical data under stable state and vibration state.

Output: stable state data set X^S, vibration state data set X^V.

Step1: Normalize data set X $(I \times J)$ and time interval $\Delta t_{ii'}(i = 1, \ldots, I, i' = 1, \ldots, I)$;

Step2: Calculate the local densities ρ and distances δ for every sample by Eq. (7) and Eq. (8).

Step3: Plot the decision diagram based on ρ and δ. In decision diagram, these samples with higher value of ρ and δ are labeled as the cluster centers.

Step4: Assign the remaining unlabeled samples to the nearest cluster center and form several clusters.

Step5: Arrange each sample in every cluster in chronological order. Divide the time continuous samples of every cluster into same stage and the time discontinuous samples of every cluster into different stages.

Step6: Calculate the mean values of samples in each stage denoted as c_r. Calculate the Euclidean distance d_{rs} between c_r and c_s. Calculate the Euclidean distance d_{rv} between c_r and c_v respectively. If $d_{rs} < d_{rv}$, samples are assigned to X^S, otherwise, are assigned to X^V.

IV. MULTI-MODEL PREDICTION METHOD FOR FLOATING HEIGHT

Based on the division results of hard division, the multi-model prediction method for floating height at stable state and vibration state is established. The multi-model frame is composed of hybrid prediction model under stable state (HPMSS) and the XGBoost-based model under vibration state (XGBMVS).

A. HYBRID PREDICTION MODEL UNDER STABLE STATE (HPMSS)

The mechanism model has the advantage of high robustness and the data driven model has the advantages of strong learning ability and favorable prediction effect. In order to combine the advantages of mechanism model and data driven model, a hybrid prediction model is established. The mechanism model is established based on force balance equation and inviscid theory, which can predict the major information of the floating height. Besides, the data driven model compensates the error of the mechanism model.

1) MECHANISM MODEL

The mechanism model of air cushion furnace with hybrid nozzles is proposed based on the force balance equation and Alexander's inviscid theory which is a type of ground effect theory. The inviscid theory of Alexander assumed that the total pressure of the air injection would not change even after it contacts with the wall [16]. Alexander's inviscid equation is:

$$\frac{p_c}{p_t} = \frac{2(1+\cos\theta)}{\frac{h}{b} + \frac{1}{2} + \cos\theta}, \tag{9}$$

where, p_c is the air cushion pressure, p_t is the pressure of the air jet after the slot nozzle, b is the width of the slot nozzle, h is the floating height of the strip, and θ is the angle of the slot nozzle.

For hybrid nozzle, it is assumed that the cushion pressure near the nozzle is not affected by the round nozzle, and only a small part of the air is discharged through the round nozzle [16]. The air impinging force per unit length is expressed as:

$$\frac{F}{bp_t} = \frac{p_c}{p_t}\left(\frac{w}{b} + \frac{h}{b}\frac{2\sin\theta}{1+\cos\theta} + \frac{L-w}{b}\frac{\Delta p_1}{p_c}\right), \tag{10}$$

where $\frac{p_c}{p_t}$ is given by Eq. (9), w indicates the distance between the two slot nozzle, L is the distance between the slot nozzle and the round nozzle, and Δp_1 represents the pressure drop between the strip and the round nozzle.

If we assume that the floating height is uniform and small, and the flow in the gap between the strip and the air box is laminar, the pressure drop Δp_1 can be expressed as:

$$\frac{\Delta p_1}{p_c} = \frac{p_*}{p_c}\left(\sqrt{1 + 2\frac{p_c}{p_*}} - 1\right), \tag{11}$$

where

$$p_* = \frac{1}{\rho}\left(\frac{3\pi N C_d d^2 \mu L}{h^3}\right), \tag{12}$$

where, ρ is the air density, N is the number of round nozzles in a row per unit length of air box, C_d is the discharge coefficient, d is the diameter of the round nozzles, and μ is dynamic viscosity of air.

According to the above analysis, the upward force on the strip can be expressed as:

$$\frac{F_U}{bp_{t1}} = \frac{p_{c1}}{p_{t1}}\left(\frac{w}{b} + \frac{h}{b}\frac{2\sin\theta}{1+\cos\theta} + \frac{L-w}{b}\frac{\Delta p_{U1}}{p_{c1}}\right), \tag{13}$$

where p_{t1} is the pressure of the air jet after the lower slot nozzle, Δp_{U1} indicates the pressure drop between the strip and the lower round nozzle, and p_{c1} is the air cushion pressure of lower surface of the strip given by Eq. (9). Similarly, the downward force on the strip can be expressed as:

$$\frac{F_D}{bp_{t2}} = \frac{p_{c2}}{p_{t2}}\left(\frac{w}{b} + \frac{D-h}{b}\frac{2\sin\theta}{1+\cos\theta} + \frac{L-w}{b}\frac{\Delta p_{D1}}{p_{c2}}\right) \tag{14}$$

where, D is the distance between the upper and lower air boxes, p_{t2} is the pressure of the upper slot nozzle, Δp_{D1} represents the pressure drop between the strip and the upper round nozzle, and p_{c2} is the air cushion pressure of the upper surface of the strip given by Eq. (9).

According to the principle of force balance, when the strip floats steadily, the sum of the downward force and the gravity of the strip itself is equal to the upward force. The formula can be expressed as:

$$F_U = F_D + G \tag{15}$$

where G is gravity of strip per unit length.

Finally, the equation (16) is obtained by substituting the Eq. (13) and Eq. (14) into Eq. (15). The floating height h can be obtained by solving the equation (16):

$$Ah^7 + Bh^6 + Ch^5 + Eh^4 + Fh^3 + Hh^2 + Ih + J = 0, \quad (16)$$

where, the parameters A, B, C, E, F, H, I, J are expressed as Eq. (17), Eq. (18), Eq. (19), Eq. (20), Eq. (21), Eq. (22), Eq. (23), and Eq. (24) as follows:

$$A = 4(L-w)b^2(1+\cos\theta)^2Q[-16D + 8b(1+2\cos\theta)], \quad (17)$$

$$B = 4(L-w)b^2(1+\cos\theta)^2Q\{-[2D + b(1+2\cos\theta)]^2 + b^2(1+2\cos\theta)^2 + 60D^2 - 24b(1+2\cos\theta)D\}, \quad (18)$$

$$C = 4(L-w)b^2(1+\cos\theta)^2Q[-6b^2(1+2\cos\theta)^2D + 60b(1+2\cos\theta)D^2 - 80D^3], \quad (19)$$

$$E = 64b\sin\theta(p_{t1} - p_{t2}) - 4(L-w)b^2(1+\cos\theta)^2 \times \left[-15b^2(1+2\cos\theta)^2D^2 + 80bQD^3(1+2\cos\theta) - 60QD^4\right] - 16G, \quad (20)$$

$$F = 32bL(1+\cos\theta)(p_{t1}+p_{t2}) + [8D + 4b(1 + 2\cos\theta)](-16b\sin\theta p_{t1} + 8b\sin\theta p_{t2} + 4G) + 16b(1+2\cos\theta)[b\sin\theta(2p_{t1} - 4p_{t2}) - G] + 4(L-w)b^2(1+\cos\theta)^2Q[-24D^5 + 60b(1 + 2\cos\theta)D^4 - 20b^2(1+2\cos\theta)^2D^3] + 64b\sin\theta Dp_{t2}, \quad (21)$$

$$H = [2D + b(1+2\cos\theta)]^2[16b\sin\theta p_{t1} - 4G] + [8D + 4b(1+2\cos\theta)][b(1+2\cos\theta)(-8b\sin\theta p_{t1} + 8b\sin\theta p_{t2} + 4G) - 8bL(1+\cos\theta)p_{t1}] + [4b(1 + 2\cos\theta) - 8D][8b\sin\theta Dp_{t2} + (1+\cos\theta)4bLp_{t2}] + [15b^2(1+2\cos\theta)^2 - 24b(1+2\cos\theta)D + 4D^2]^2 \times QD^4 4(L-w)b^2(1+\cos\theta) - b^2(1+2\cos\theta)^2[16b \times \sin\theta p_{t2} + 4G] + 16b^2L(1+\cos\theta)(1+2\cos\theta)p_{t1}, \quad (22)$$

$$I = [2D + b(1+2\cos\theta)]^2[8bL(1+\cos\theta)p_{t1} + 4b(1 + 2\cos\theta)(2b\sin\theta p_{t1} - G)] + b(1+2\cos\theta)[8D + 4b(1+2\cos\theta)][-4L(1+\cos\theta)p_{t1} + 2b\sin\theta(1 + 2\cos\theta)p_{t2} - 8D\sin\theta p_{t2} - 4L(1+\cos\theta)p_{t2} + (1 + 2\cos\theta)G] + b^2(1+2\cos\theta)^2[16bD\sin\theta p_{t2} + 8 \times bL(1+\cos\theta)p_{t2} - 24(L-w)b^2(1+\cos\theta)^2QD^5] + 16b^3(1+2\cos\theta)(L-w)(1+\cos\theta)^2QD^6, \quad (23)$$

$$J = -b^2(1+2\cos\theta)^2[2D + b(1+2\cos\theta)][8b\sin\theta Dp_{t2} + 4bL(1+\cos\theta)p_{t2} + G] + 4b^2L(1+\cos\theta)(1 + + 2\cos\theta)p_{t1}[2D + b(1+2\cos\theta)]^2 4(L-w)b^4QD^6 (1+\cos\theta)^2(1+2\cos\theta)^2. \quad (24)$$

The parameter Q in Eq. (17), Eq. (18), Eq. (19), Eq. (20), Eq. (21), Eq. (22), Eq. (23), and Eq. (24) is specified as:

$$Q = \rho \Big/ (3\pi NC_d d^2 \mu L)^2. \quad (25)$$

2) XGBOOST ERROR COMPENSATION MODEL

There exists an error between the actual floating height and the prediction value of the mechanism model. The XGBoost [33] has the advantage of high prediction accuracy and robustness to outliers, so the XGBoost is used to compensate the error of the mechanism model. The training process for the XGBoost error compensation model is shown in Fig. 5.

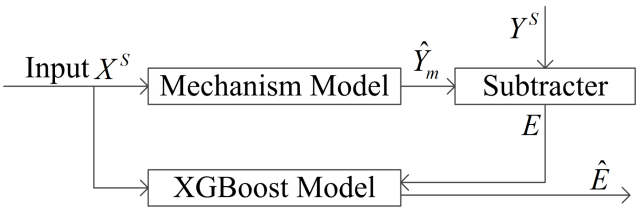

FIGURE 5. The training process of the XGBoost error compensation model.

The training process of XGBoost error compensation model is shown as Fig. 5. Firstly, X^S is input to the mechanism model and the output value $\hat{Y}_m$ of the mechanism model is obtained. Secondly, E is the difference between the prediction value $\hat{Y}_m$ of the mechanism model and the actual floating height Y^S. Thirdly, the dataset $\{X^S, E\}$ is established as the training set for the XGBoost model. Finally, the XGBoost error compensation model is used to predict the error $\hat{E}$ of the mechanism model.

3) HYBRID PREDICTION MODEL

The hybrid prediction model is consisted of mechanism model and XGBoost model. The mechanism model predicts the major information of floating height and the XGBoost model compensates the error between the prediction value of the mechanism model and the actual value. The schematic diagram of the hybrid prediction model is shown in Fig. 6.

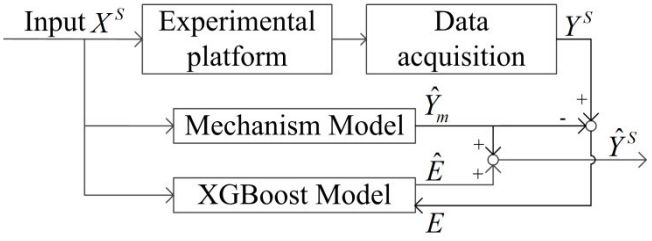

FIGURE 6. Schematic diagram of the hybrid prediction model.

As shown in Fig. 6, the prediction process of floating height at stable state is shown as follows:

(1) Input X^S to the air cushion experimental platform with hybrid nozzles and Y^S is collected by sensors during the data acquisition process.

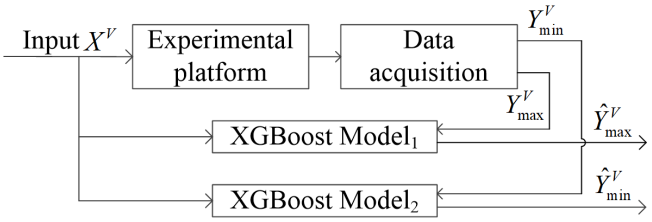

FIGURE 7. Schematic diagram of XGBoost-based model under vibration state.

(2) Input variable X^S to the mechanism model and obtain the prediction value $\hat{Y}_m$ of the mechanism model. Train the XGBoost error compensation model.

(3) The predicted floating height $\hat{Y}^S$ is obtained by adding the predicted value of the mechanism model and the predicted error of the XGBoost error compensation model.

B. XGBOOST-BASED MODEL UNDER VIBRATION STATE (XGBMVS)

At vibration state, the strip is more likely to vibrate up and down. There exist fluid and solid coupling process and physical theory is extremely complex and it is hard to establish a mechanism model for such a complicate floating process. The strip may contact with the furnace easily at vibration state and be scratched when the strip is at the maximum or minimum positions. Therefore, the maximum and minimum heights are two key values for the production process. Due to the strong learning ability of the XGBoost model, it is selected to predict the maximum and minimum floating heights at vibration state.

The prediction process of floating height model for vibration state is shown in Fig. 7. At first step, the maximum and minimum height values $Y^V_{\max}$, $Y^V_{\min}$ are collected by data acquisition procedure. At the second step, the data set $\left(X^V, Y^V_{\max}\right)$ is used to train the XGBoost$_1$ model and the training set $\left(X^V, Y^V_{\min}\right)$ is used to train the XGBoost$_2$ model. Finally, the predicted maximum floating height $\hat{Y}^V_{\max}$ and minimum floating height $\hat{Y}^V_{\min}$ are obtained by XGBoost$_1$ and XGBoost$_2$ model respectively.

C. HARD-DIVISION AND MULTI-MODEL BASED FLOATING HEIGHT PREDICTION FRAMEWORK

The framework of hard-division and multi-model based floating height prediction method is shown in Fig. 8. The general procedure of the method is as follows:

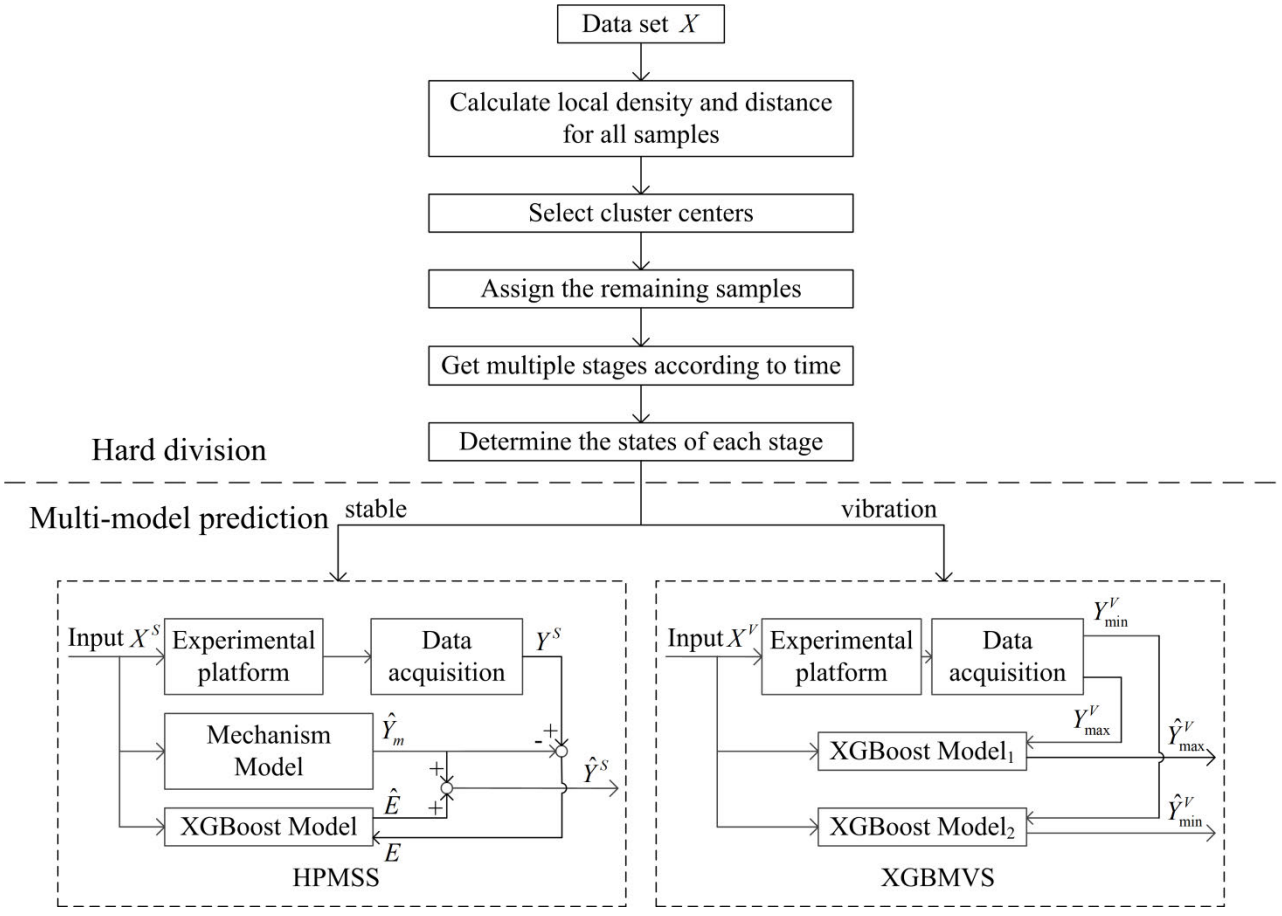

FIGURE 8. The framework of hard-division and multi-model based floating height prediction method.

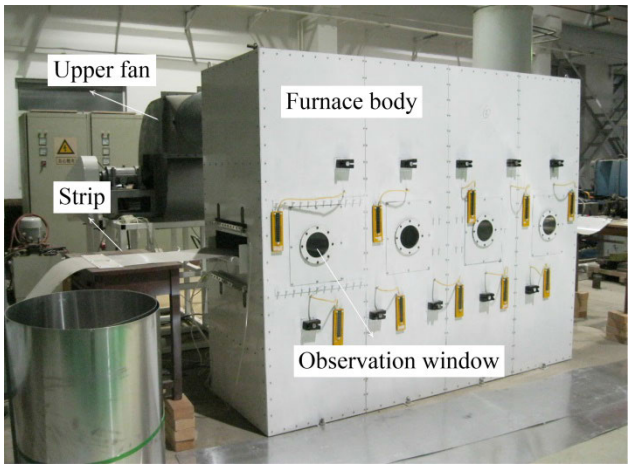

FIGURE 9. The physical diagram of air cushion experimental platform with hybrid nozzles.

Step 1: The data set X during the process is divided into several segments. Each segment is labeled by stable stage or vibration stage. Details about TICMDC-HD are described in section III. The sketch map of this step can also be seen on the hard division part of Fig. 8.

Step 2: Based on the division result of Step1, if the data sets are labeled by stable stage, go to Step 3. Otherwise, go to Step 4.

Step 3: Input the data set labeled by stable stage into HPMSS and the prediction value of floating height in stable stage can be obtain. This step is described in section IV-A and can also be seen on the left bottom of Fig. 8.

Step 4: Input the data set labeled by vibration stage into XGBMVS and the prediction maximum and minimum values of floating height in vibration stage can be got. This step is described in section IV-B and can also be seen on the right bottom of Fig. 8.

Step 5: Output the prediction values of the floating height on Step 3 and Step 4.

V. EXPERIMENTS AND ANALYSIS

A. AIR CUSHION FURNACE EXPERIMENTAL PLATFORM

In order to validate the effectiveness of the hard-division and multi-model based floating height prediction method, an amount of experiments are carried out on the air cushion furnace experimental platform with hybrid nozzles. The specification of air cushion furnace experimental platform is 3m $\times$3m $\times$2.2m. The experimental platform of the air cushion furnace is mainly composed of the furnace body, the air seal device, the upper fan, the lower fan, the upper air container, the lower air container, the upper nozzles and the lower nozzles. There are three types of nozzles, including double slot nozzles, hybrid nozzles and round nozzles. The type of nozzles can be changed according the requirement of experiment. In this article, the experiment is carried out based on the hybrid nozzles. For convenience, the physical diagram and the structure diagram of air cushion furnace experimental platform are shown in Fig. 9 [15] and Fig. 10, respectively.

The speed of upper fan and the lower fan is adjusted by the Siemens frequency converter MM 440. The pressure in upper hybrid nozzles and lower hybrid nozzles is changed with the speed of upper fan and lower fan. The laser rangefinder LOD2-250W150 with measuring accuracy and range of 75 μm and 100mm-400mm is used in the experimental process of the air cushion furnace to measure the floating height of the strip, respectively.

B. EXPERIMENTAL SETUP

Two kinds of strips are used in the experimental process. The width of the strips is 400mm and the thickness of the strips is 1mm and 1.5mm, respectively. 1920 samples were collected to form a total dataset in the experimental process. The total dataset includes 880 samples under stable state and 1040 samples under vibration state. 24 samples under four stable states and 48 samples under four vibration states are selected as the test samples for hybrid prediction model and XGBoost-based model.

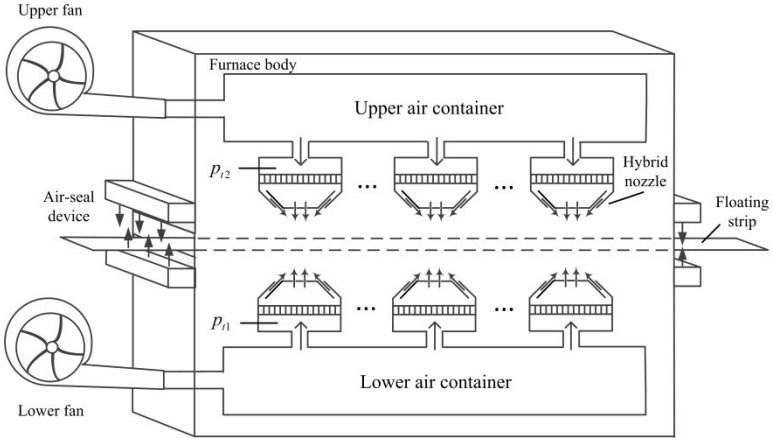

FIGURE 10. The structure diagram of air cushion furnace experimental platform.

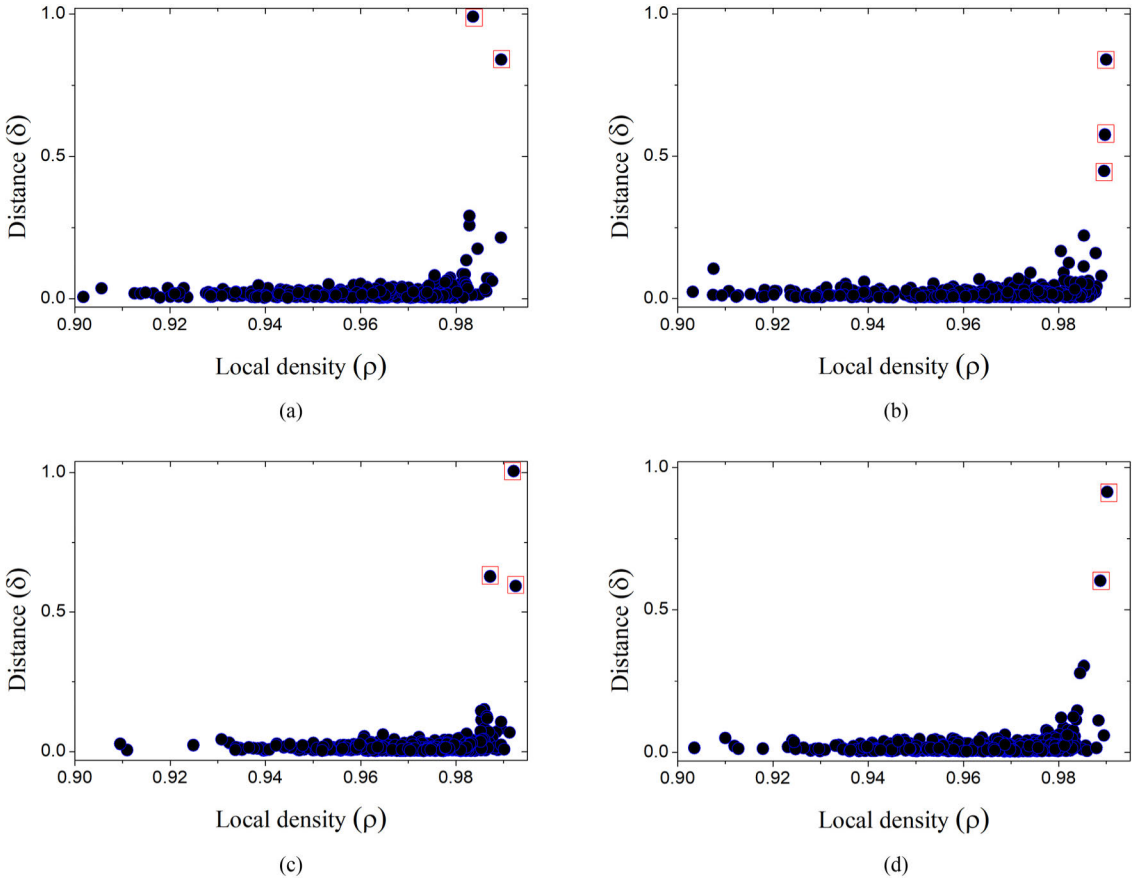

FIGURE 11. Decision graphs: (a) thickness = 1.0mm, p_{t2} = 200Pa; (b) thickness = 1.0mm, p_{t2} = 380Pa; (c) thickness = 1.5mm, p_{t2} = 200Pa; (d) thickness = 1.5mm, p_{t2} = 380Pa.

The precision of the model affects the quality of the model. The MAE, RMSE and MAPE are common evaluation indicators for the prediction performance of machine learnings. These evaluation indicators are also used to verify the effectiveness of the model in this article. The equations of MAE, RMSE and MAPE are respectively given as:

$$MAE = \frac{1}{n}\sum_{i=1}^{n}\left|\hat{y}_i - y_i\right|, \tag{26}$$

$$RMSE = \sqrt{\frac{1}{n}\sum_{i=1}^{n}\left(\hat{y}_i - y_i\right)^2}, \tag{27}$$

$$MAPE = \frac{100}{n}\sum_{i=1}^{n}\left|\frac{\hat{y}_i - y_i}{y_i}\right|, \tag{28}$$

where, y_i is the actual value of the height and $\hat{y}_i$ is the predicted value of the height. The smaller the MAE, RMSE, and MAPE are, the higher the prediction accuracy is.

C. EXPERIMENTAL RESULTS AND DISCUSSION

1) RESULTS OF TICMDC-HD

The data set X is collected in the procedure of experimental process under four conditions. The process variables of sample are the pressure values of upper nozzles, the pressure values of lower nozzles, the thickness of strip, the speed of upper fan, the speed of lower fan. Four conditions are studied. The conditions are: (a) thickness = 1.0mm, p_{t2} = 200Pa; (b) thickness = 1.0mm, p_{t2} = 380Pa; (c) thickness = 1.5mm, p_{t2} = 200Pa; and (d) thickness = 1.5mm, p_{t2} = 380Pa.

The samples in the dataset are divided and recognized by the hard division method. The decision graphs of experimental results under four conditions are established and shown in Fig. 11. In Fig. 11, the lateral axis is local density ρ and vertical axis is δ. As shown in Fig. 11(a), (b), (c), and (d), the samples with large local density and distance are defined as the cluster center. In order to observe conveniently, the cluster centers are marked by red box. The samples in the dataset are divided into stable state and vibration state as shown in Fig. 12.

In Fig. 12, the lateral axis is sample points collected in time series and the vertical axis is the number of stages. In order to observe conveniently, the cluster centers are marked by red color. In Fig. 12(a), the conditions in actual process vary from stable condition to vibration condition. The samples in the process are divided into two stages, i.e., 1-200 and 201-480. The first stage is identified as the stable state. The second

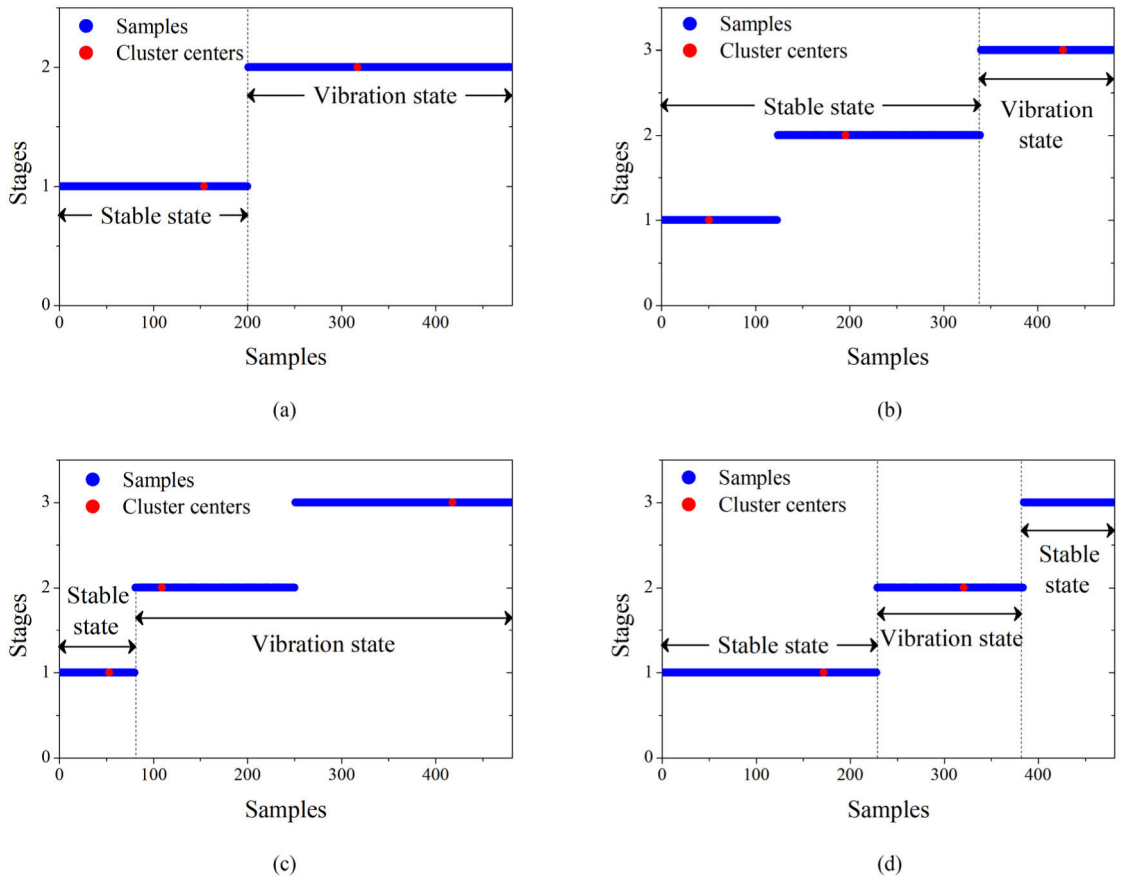

FIGURE 12. The result of the hard division method: (a) thickness = 1.0mm, p_{t2} = 200Pa; (b) thickness = 1.0mm, p_{t2} = 380Pa; (c) thickness = 1.5mm, p_{t2} = 200Pa; (d) thickness = 1.5mm, p_{t2} = 380Pa.

stage is identified as vibration state. Each stage has a cluster center.

In Fig. 12(b), the conditions in actual process vary from two different stable conditions to vibration condition. The samples are divided into three stages, 1-123, 124-339, and 340-480, respectively. The first two stages are identified as the stable state. The third stage is identified as vibration state. Each stage has a cluster center.

In Fig. 12(c), the conditions in actual process vary from one stable condition to two different vibration conditions. The samples in the process are divided into three stages, 1-80, 81-250, and 251-480, respectively. The first stage is identified as the stable state. The second and third stages are identified as vibration state.

In Fig. 12(d), three conditions exist in the actual process. Two transition processes exist in actual process. In the first transition process, the conditions in actual process vary from one stable condition to vibration condition. In the second transition process, the conditions in actual process vary from vibration condition to stable condition. The samples in the process are divided into three stages, 1-228, 229-384, and 385-480, respectively. The first stage is identified as the stable state. The second stage is identified as vibration state. The third stage is identified as stable state. A phenomenon can be found in Fig. 12(d), two cluster centers exist in the first stable stage and vibration stage. The final stage does not own cluster center. The reason is as follow: the experimental equipment in the first and the third stages works at same working condition under stable state. Duo to the requirement of working process, a vibration stage is inserted between the first stable stage and second stable stage. The first and the final stages with same working condition should be clustered into same cluster and the first and final stages own same cluster. However, the time sequence of first and the final stages is discontinuous, so the first and final stages are divided into two different stages.

2) EXPERIMENTAL RESULT OF HPMSS

In order to verify the hybrid prediction model, firstly, three comparison methods including the mechanism model (MM), the XGBoost model and the support vector regression (SVR) model are provided. Secondly, the hybrid prediction model is tested under four conditions. The four conditions are: (a) thickness = 1.0mm, p_{t2} = 200Pa; (b) thickness = 1.0mm, p_{t2} = 380Pa; (c) thickness = 1.5mm, p_{t2} = 200Pa; (d) thickness = 1.5mm, p_{t2} = 380Pa. The experimental results are shown in Fig. 13.

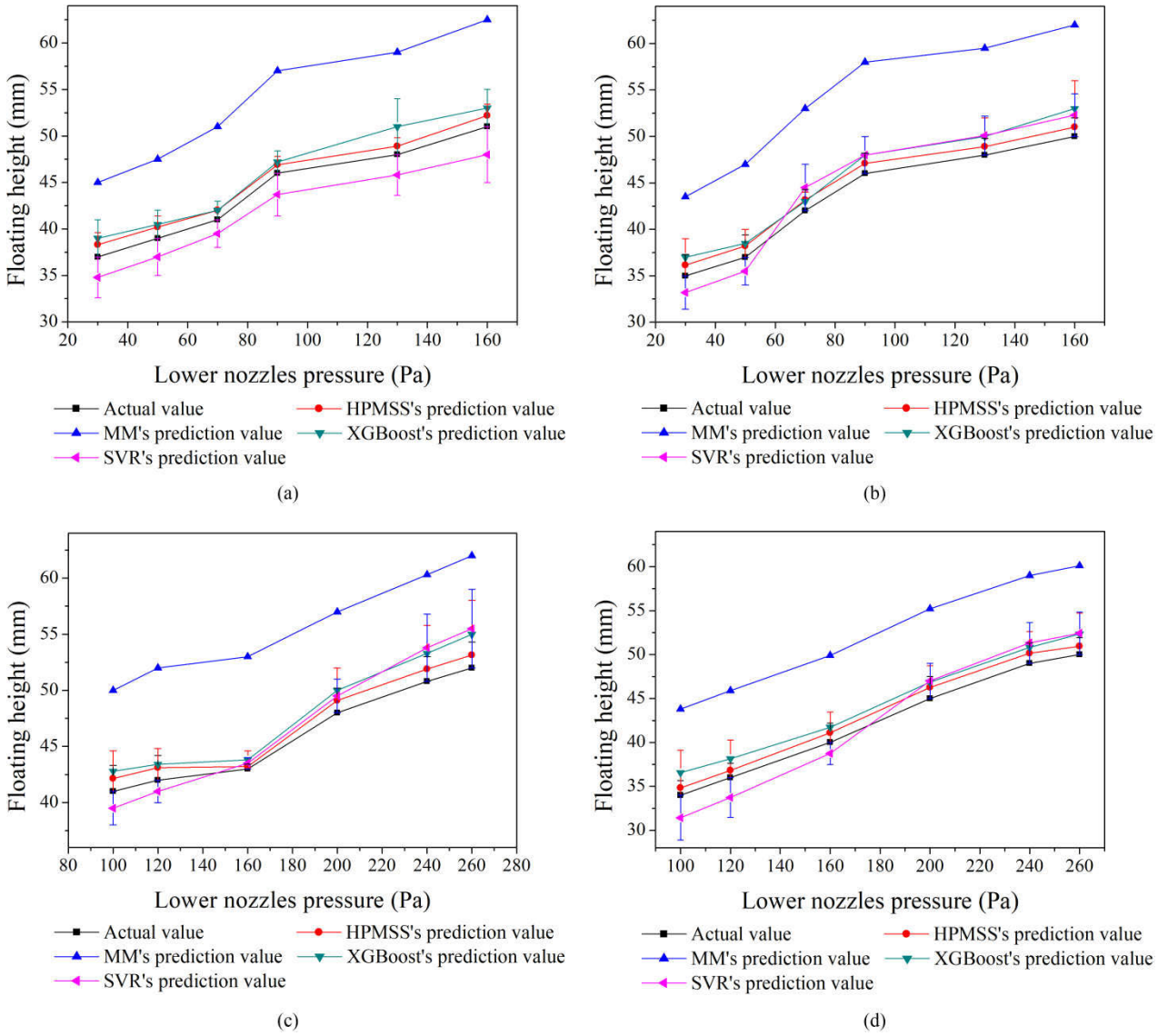

FIGURE 13. Quantitative comparison of different prediction models and actual prediction height at stable state: (a) thickness = 1.0mm, p_{t2} = 200Pa; (b) thickness = 1.0mm, p_{t2} = 380Pa; (c) thickness = 1.5mm, p_{t2} = 200Pa; (d) thickness = 1.5mm, p_{t2} = 380Pa.

TABLE 2. Comparison of the MAE for different models at stable state.

Algorithm	1.0mm, 200Pa	1.0mm, 380Pa	1.5mm, 200Pa	1.5mm, 380Pa	Total
MM	10.000	10.833	9.583	9.983	40.400
XGBoost	1.783	1.917	1.917	2.072	7.689
SVR	2.200	2.033	1.833	2.136	8.203
HPMSS	**1.083**	**1.083**	**0.967**	**1.017**	**4.150**

TABLE 3. Comparison of the RMSE for different models at stable state.

Algorithm	1.0mm, 200Pa	1.0mm, 380Pa	1.5mm, 200Pa	1.5mm, 380Pa	Total
MM	10.087	10.905	9.594	9.984	40.570
XGBoost	1.901	2.010	2.045	2.094	8.051
SVR	2.244	2.059	2.121	2.179	8.604
HPMSS	**1.095**	**1.088**	**1.026**	**1.030**	**4.238**

In order to observe conveniently, the MAE, RMSE and MAPE values of the four algorithms are shown in Table 2, Table 3, and Table 4 respectively. The smaller the MAE, RMSE and MAPE are, the better effect the algorithm is. The algorithm with best effect is shown in bold front.

As shown in Table 2, Table 3, and Table 4, the MAE, RMSE and MAPE values of the mechanism model are significantly bigger than other models under the four working conditions. The reasons may be that the mechanism model is constructed on several ideal assumptions. But the fluid and solid coupling

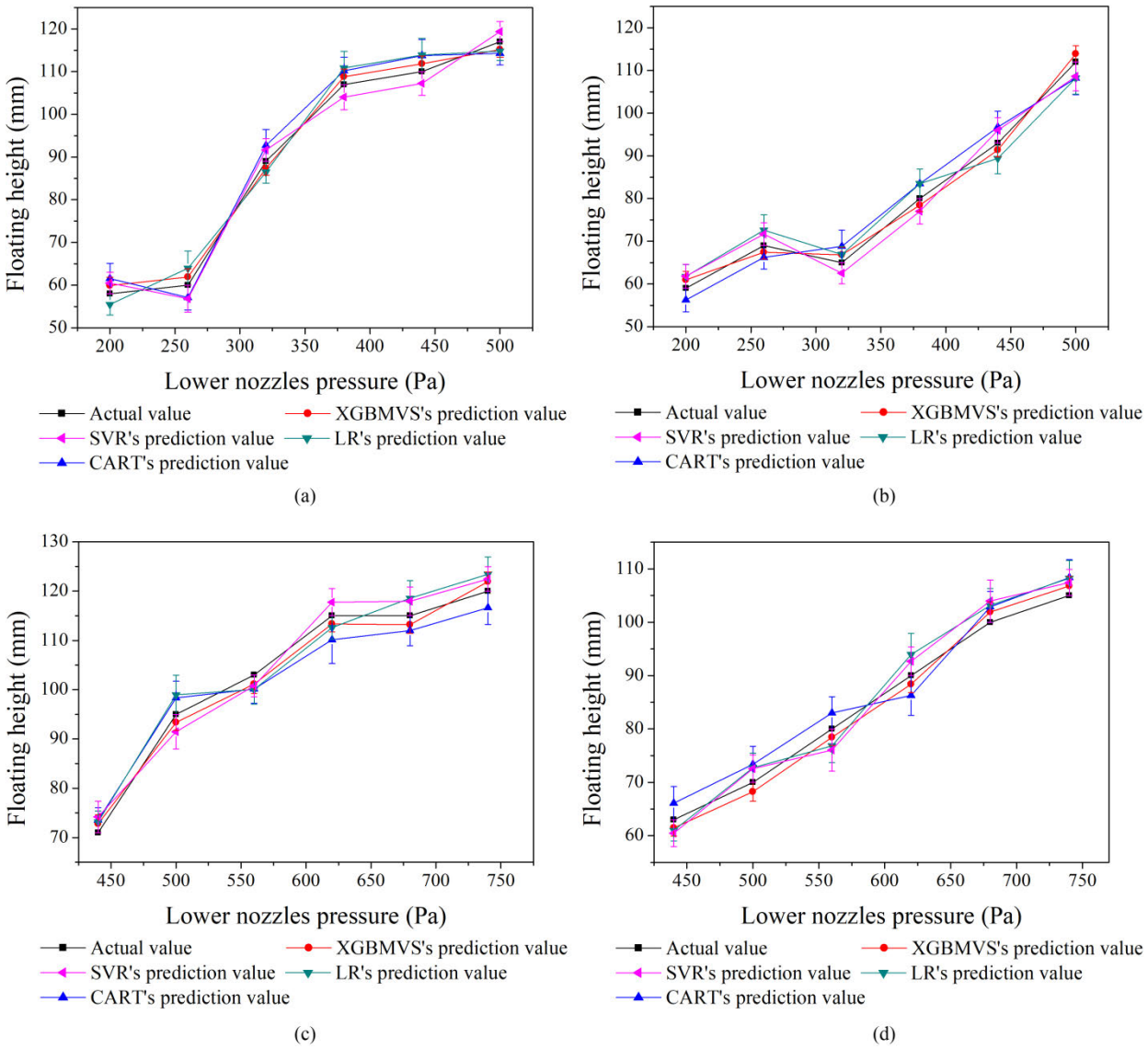

FIGURE 14. The minimum floating height prediction results of the XGBoost-based model under vibration state: (a) thickness = 1.0mm, p_{t2} = 200Pa; (b) thickness = 1.0mm, p_{t2} = 380Pa; (c) thickness = 1.5mm, p_{t2} = 200Pa; (d) thickness = 1.5mm, p_{t2} = 380Pa.

TABLE 4. Comparison of the MAPE for different models at stable state.

Algorithm	1.0mm, 200Pa	1.0mm, 380Pa	1.5mm, 200Pa	1.5mm, 380Pa	Total
MM	22.864	25.258	20.950	24.058	93.130
XGBoost	4.079	4.444	4.074	5.047	17.643
SVR	5.033	4.745	3.827	5.162	18.768
HPMSS	**2.536**	**2.589**	**2.093**	**2.416**	**9.633**

process in actual process is complex and the state of the actual process is non-ideal.

The values of MAE, RMSE and MAPE for XGBoost model and SVR model are smaller than the mechanism model. The reasons may be that the data driven model has strong learning ability and can reflect the potential relationship between samples. In addition, the values of MAE, RMSE and MAPE of XGBoost model are smaller than SVR. The causes may be that the XGBoost is a kind of ensemble algorithm which integrates multiple learners and has stronger learning ability. Finally, the values of MAE, RMSE and MAPE for HPMSS model are smaller than other three algorithms. The reasons may be that the mechanism model has advantage of generalization ability and the data model has strong learning ability. The HPMSS model is a kind of hybrid model which combines the advantages of mechanism model and data driven model. So the prediction performance of the HPMSS model is better than MM, SVR and XGBoost.

Conditions at vibration state. The four conditions are: (a) thickness = 1.0mm, p_{t2} = 200Pa; (b) thickness = 1.0mm, p_{t2} = 380Pa; (c) thickness = 1.5mm, p_{t2} = 200Pa;

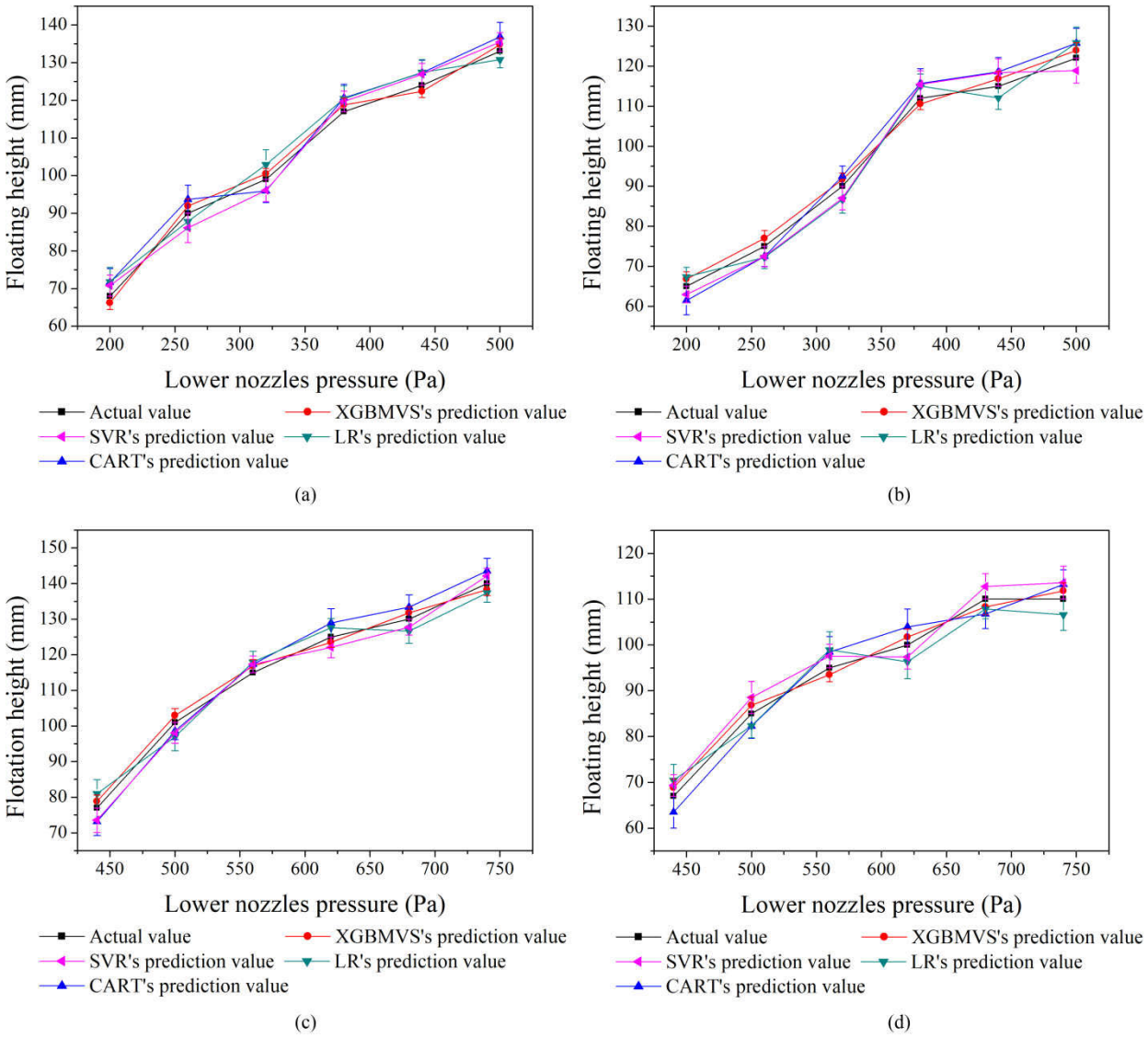

FIGURE 15. The maximum floating height prediction results of the XGBoost-based model under vibration state: (a) thickness = 1.0mm, p_{t2} = 200Pa; (b) thickness = 1.0mm, p_{t2} = 380Pa; (c) thickness = 1.5mm, p_{t2} = 200Pa; (d) thickness = 1.5mm, p_{t2} = 380Pa.

TABLE 5. Comparison of the MAE for different models at vibration state.

Algorithm	Minimum value					Maximum value				
	1.0mm, 200Pa	1.0mm, 380Pa	1.5mm, 200Pa	1.5mm, 380Pa	Total	1.0mm, 200Pa	1.0mm, 380Pa	1.5mm, 200Pa	1.5mm, 380Pa	Total
SVR	2.730	2.882	2.850	3.024	11.486	2.954	2.925	2.667	2.907	11.453
LR	3.163	3.181	3.092	3.046	12.482	3.160	3.052	3.256	3.206	12.674
CART	3.315	3.392	3.336	3.245	13.288	3.552	3.270	3.257	3.330	13.409
XGBMVS	**1.815**	**1.737**	**1.780**	**1.695**	**7.027**	**1.729**	**1.771**	**1.750**	**1.738**	**6.988**

(d) thickness = 1.5mm, p_{t2} = 380Pa. The prediction results of the minimum floating height and maximum floating height are shown in Fig. 14 and Fig. 15, respectively.

In order to observe conveniently, the values of MAE, RMSE and MAPE of XGBMVS and other three models are shown in Table 5, Table 6, and Table 7, respectively. It is obvious that the values of MAE, RMSE and MAPE of XGBMVS are smaller than others. It indicates that the predicted values of XGBMVS are very close to the actual values in the floating height prediction of the strip under vibration state. This verifies the effectiveness of XGBMVS in predicting the floating height of strip under vibration state.

TABLE 6. Comparison of the RMSE for different models at vibration state.

Algorithm	Minimum value					Maximum value				
	1.0mm, 200Pa	1.0mm, 380Pa	1.5mm, 200Pa	1.5mm, 380Pa	Total	1.0mm, 200Pa	1.0mm, 380Pa	1.5mm, 200Pa	1.5mm, 380Pa	Total
SVR	2.743	2.900	2.883	3.100	11.626	2.987	2.966	2.709	2.945	11.607
LR	3.254	3.248	3.157	3.102	12.761	3.241	3.089	3.306	3.266	12.902
CART	3.340	3.423	3.416	3.257	13.436	3.561	3.312	3.323	3.352	13.548
XGBMVS	**1.818**	**1.745**	**1.784**	**1.701**	**7.048**	**1.736**	**1.780**	**1.756**	**1.742**	**7.014**

TABLE 7. Comparison of the MAPE for different models at vibration state.

Algorithm	Minimum value					Maximum value				
	1.0mm, 200Pa	1.0mm, 380Pa	1.5mm, 200Pa	1.5mm, 380Pa	Total	1.0mm, 200Pa	1.0mm, 380Pa	1.5mm, 200Pa	1.5mm, 380Pa	Total
SVR	3.303	3.732	2.895	3.651	13.581	2.991	3.078	2.499	3.130	11.698
LR	3.806	4.065	3.037	3.616	14.524	3.224	3.245	3.041	3.519	13.029
CART	3.987	4.383	3.258	3.958	15.586	3.561	3.524	2.962	3.630	13.677
XGBMVS	**2.200**	**2.294**	**1.780**	**2.052**	**8.326**	**1.738**	**1.947**	**1.598**	**1.905**	**7.188**

VI. CONCLUSION

In this article, a hard-division and multi-model based floating height prediction method for air cushion furnace with hybrid nozzles is proposed. Several conclusions are obtained as follows:

1) A hard-division and multi-model based floating height prediction method for air cushion furnace with hybrid nozzles is proposed. This method can divide the process into stable state and vibration state. Besides, it can predict the floating height at stable state and vibration state.
2) In order to avoid the wrong division caused by noise and improve the information capture ability for dynamic process, a time interval and covariance matrices density clustering based hard division method is proposed. This novel hard division method can divide the process into stable state and vibration state successfully.
3) For the stable state of air cushion furnace with hybrid nozzles, a novel hybrid model combining mechanism model and data driven model is presented. The mechanism model is proposed based on the force balance equation and inviscid theory. The data driven model is established by XGBoost model. The mechanism model predict the major information of floating height and the data driven model is used to compensate the error between the mechanism model and actual value. The experimental results show that the hybrid model can get higher prediction accuracy than the mechanism model, the XGBoost model and the SVR algorithm.
4) Under vibration state, the maximum and the minimum floating height XGBoost models are established to predict the maximum and minimum floating height respectively, and get desirable prediction results.

The content of this article lays a theoretical foundation for state division and floating height prediction in the air cushion furnace with hybrid nozzles. In addition, it has important application value for the high-efficiency and high-quality production of the industry process.

However, the method proposed in this article only suitable for the air cushion furnace with hybrid nozzles and it is not suitable for the air cushion furnace with double slot nozzles or round nozzles. We will explore a method which can be used in a wide range of scenarios in future.

REFERENCES

[1] H. T. Sun, J. Wang, G. Z. Shen, and P. Hu, "Application of warm forming aluminum alloy parts for automotive body based on impact," *Int. J. Automot. Technol.*, vol. 14, no. 4, pp. 605–610, Aug. 2013.
[2] C. Sasse, F. Brühl, and M. Schäfer, "Thermal treatment of aviation aluminum alloys in strip processing lines," *Key Eng. Mater.*, vol. 746, pp. 168–175, Jul. 2017.
[3] Y. Y. Woo, S. W. Han, J. R. Cho, and Y. H. Moon, "Air jet impingement to reduce hot strip wave on a run-out table," *Mech. Ind.*, vol. 19, no. 6, p. 601, 2018.
[4] Y. Li, Z. Wang, M. Ma, G. Wang, T. Fu, J. Li, and X. Liang, "The air cushion furnace technology for heat treatment of high quality aluminium alloy auto body," *Engineering*, vol. 12, no. 5, pp. 73–80, 2014.
[5] Y. Shi, M. B. Ray, and A. S. Mujumdar, "Effect of large temperature differences on local nusselt number under turbulent slot impingement jet," *Drying Technol.*, vol. 20, no. 9, pp. 1803–1825, Jan. 2002.
[6] Q. Guo, Z. Wen, and R. Dou, "Experimental and numerical study on the transient heat-transfer characteristics of circular air-jet impingement on a flat plate," *Int. J. Heat Mass Transf.*, vol. 104, pp. 1177–1188, Jan. 2017.
[7] M.-Y. Wen and K.-J. Jang, "An impingement cooling on a flat surface by using circular jet with longitudinal swirling strips," *Int. J. Heat Mass Transf.*, vol. 46, no. 24, pp. 4657–4667, Nov. 2003.
[8] C. Kramer and T. Kramer, "New developments continuous heat treatment of floatingly and touchless guided metal strips of topper alloys," *Metall*, vol. 58, no. 3, pp. 121–124, 2004.
[9] S. Hou, F. Hua, W. Lv, Z. Wang, Y. Liu, and G. Wang, "Hybrid modeling of flotation height in air flotation oven based on selective bagging ensemble method," *Math. Problems Eng.*, vol. 2013, pp. 1–9, Jan. 2013.

[10] M. Takeda and M. Watanabe, "Self-excited vibration of a plate supported by air pressure in a floating conveying machine," in *Proc. Fluid-Struct. Interact.*, vol. 4, Jul. 2017, Art. no. V004T04A035.
[11] K. Hornig, R. Blling, H. J. Odenthal, H. Pfeifer, and K. Schmitz, "Simulation of fluid flow and strip stability in a strip floatation furnace by physical and numerical methods," in *Proc. 6th Thermo Process Conf.*, 2003, pp. 1–18.
[12] P. M. Moretti, "Lateral deflections of Webs in air-flotation ovens," *J. Appl. Mech.*, vol. 71, no. 3, pp. 314–320, May 2004.
[13] C. Hyun-Ki, "Flow-induced vibration of a Web floating over a pressure-pad air bar," Ph.D. dissertation, Dept. Mech. Eng., Oklahoma State Univ., Stillwater, OK, USA, 2005.
[14] S. Hou, J. Liu, and W. Lv, "Flotation height prediction under stable and vibration states in air cushion furnace based on hard division method," *Math. Problems Eng.*, vol. 2019, pp. 1–14, Dec. 2019.
[15] S. Hou, X. Zhang, W. Dai, X. Han, and F. Hua, "Multi-model- and soft-transition-based height soft sensor for an air cushion furnace," *Sensors*, vol. 20, no. 3, p. 926, Feb. 2020.
[16] Y. B. Chang and P. M. Moretti, "Aerodynamic characteristics of pressure-pad air bars," *J. Appl. Mech.*, vol. 67, no. 1, pp. 177–182, Mar. 2000.
[17] Y. Yang, Q. Zeng, G. Yin, and L. Wan, "Vibration test of single coal gangue particle directly impacting the metal plate and the study of coal gangue recognition based on vibration signal and stacking integration," *IEEE Access*, vol. 7, p. 106 784-106 805, 2019.
[18] A. Senderovich, C. D. Francescomarino, C. Ghidini, K. Jorbina, and F. M. Maggi, "Intra and inter-case features in predictive process monitoring: A tale of two dimensions," in *Proc. Int. Conf. Bus. Process Manage.*, 2017, pp. 306–323.
[19] D.-K. Choi, "Data-driven materials modeling with XGBoost algorithm and statistical inference analysis for prediction of fatigue strength of steels," *Int. J. Precis. Eng. Manuf.*, vol. 20, no. 1, pp. 129–138, Jan. 2019.
[20] Z. Que and Z. Xu, "A data-driven health prognostics approach for steam turbines based on XGBoost and DTW," *IEEE Access*, vol. 7, pp. 93131–93138, 2019.
[21] C. Zhao and Y. Sun, "Step-wise sequential phase partition (SSPP) algorithm based statistical modeling and online process monitoring," *Chemometric Intell. Lab. Syst.*, vol. 125, pp. 109–120, Jun. 2013.
[22] Y. Qin, C. Zhao, and F. Gao, "An iterative two-step sequential phase partition (ITSPP) method for batch process modeling and online monitoring," *AIChE J.*, vol. 62, no. 7, pp. 2358–2373, Jul. 2016.
[23] M. Du, S. Ding, and H. Jia, "Study on density peaks clustering based on k-nearest neighbors and principal component analysis," *Knowl.-Based Syst.*, vol. 99, pp. 135–145, May 2016.
[24] R. Guo, N. Zhang, J. Wang, and J. Dong, "Phase partition and identification based on a two-step method for batch process:," *Trans. Inst. Meas. Control*, vol. 40, no. 16, pp. 4472–4483, 2018.
[25] J. Wang, H. Wei, L. Cao, and Q. Jin, "Soft-transition sub-PCA fault monitoring of batch processes," *Ind. Eng. Chem. Res.*, vol. 52, no. 29, pp. 9879–9888, Jul. 2013.
[26] F. Ali, U. Atila, R. Abu-Issa, and F. Murtagh, "A novel data clustering algorithm based on gravity center methodology," *Expert Syst. Appl.*, vol. 156, Oct. 2020, Art. no. 113435.
[27] D. N. Pinheiro, D. Aloise, and S. J. Blanchard, "Convex fuzzy k-medoids clustering," *Fuzzy Sets Syst.*, vol. 389, pp. 66–92, 2020, doi: 10.1016/j.fss.2020.01.001.
[28] S. Zhou, Z. Xu, and F. Liu, "Method for determining the optimal number of clusters based on agglomerative hierarchical clustering," *IEEE Trans. Neural Netw. Learn. Syst.*, vol. 28, no. 12, pp. 3007–3017, Dec. 2017.
[29] H. Li, X. Liu, T. Li, and R. Gan, "A novel density-based clustering algorithm using nearest neighbor graph," *Pattern Recognit.*, vol. 102, Jun. 2020, Art. no. 107206.
[30] J. Naveen, P. J. A. Alphonse, and S. Chinnasamy, "3D grid clustering scheme for wireless sensor networks," *J. Supercomput.*, vol. 76, no. 6, pp. 4199–4211, 2018.
[31] M. D. Parmar, W. Pang, D. Hao, J. Jang, W. Liupu, and Y. Zhou, "Fredpc: A feasible residual error-based density peak clustering algorithm with the fragment merging strategy," *IEEE Access*, vol. 7, p. 89 789-89 804, 2019.
[32] A. Rodriguez and A. Laio, "Clustering by fast search and find of density peaks," *Science*, vol. 344, no. 6191, pp. 1492–1496, Jun. 2014.
[33] T. Chen and C. Guestrin, "XGBoost: A scalable tree boosting system," in *Proc. 22nd ACM SIGKDD Int. Conf. Knowl. Discovery Data Mining*, Aug. 2016, pp. 785–794.